Journal of Structural Geology, Vol. 6, No. 1/2, pp. 121 to 133, 1984
Printed in Great Britain

0191-8141/84 $03.00 + 0.00
Pergamon Press Ltd.

Origin and significance of compositional layering in Late Precambrian sediments, Blue Ridge Province, North Carolina, U.S.A.

STEVEN E. BOYER

SOHIO Petroleum Co., 1801 California St., Denver, CO 80202, U.S.A.

(*Accepted in revised form* 29 *June* 1983)

Abstract—Basal arkosic sandstones of the Late Precambrian Grandfather Mountain Formation contain small-scale deformation zones, usually 1 mm thick and spaced 5 to 10 mm apart. The deformation zones are composed of green phengitic muscovite which concentrated in the deformation zones during pressure-solution removal of quartz. Assuming plane strain, the deformation zones have lost 34% of their area due to solution of quartz, and axial ratios of strain ellipses are on the order of 16:1 in the principal plane. The deformation zones and associated tight to isoclinal folds in the basal arkoses form a structural style which is transitional between ductile deformation zones in the crystalline basement and kink-style folding in the interbedded siltstones and arkoses of the upper Grandfather Mountain Formation.

Since deformation zones may be more common in sedimentary rocks and low-grade metasediments than previously realized, one should exercise caution when using penetrative fabrics to unravel the structural history of multiply deformed rocks. Small-scale deformation zones can be misinterpreted as a crenulation cleavage cutting an earlier penetrative fabric.

INTRODUCTION

SMALL-scale compositional layering is well-developed within Late Precambrian arkosic sandstones of the North Carolina Blue Ridge Province (Bryant & Reed 1970, pp. 76–77). Initial field observations suggested that the layering was parallel to cleavage (as defined by the microscopic alignment of micacious minerals and fibrous quartz overgrowths). Such relationships are not uncommon and can be explained by metamorphic differentiation along cleavage (Voll 1960, Nicholson 1968, Talbot & Hobbs 1968, Williams 1972). However, subsequent inspection of hand specimens and thin-sections indicated that the penetrative cleavage was frequently at a measurable angle to the layering, necessitating a new explanation for the layering (Boyer 1978, 1982a,b).

The compositionally layered arkoses occur within the Grandfather Mountain Window of northwest North Carolina (Fig. 1). The window is the product of erosion through the gently folded, one-billion-year-old crystalline basement of the Linville Falls thrust sheet (Fig. 2a) (Bryant & Reed 1970). Movement on the minor imbricate faults within the window and major thrusts beneath the window has folded the Linville Falls thrust and is thus responsible for the formation of the Grandfather Mountain Window (Boyer 1976, 1978, pp. 47–122, Boyer & Elliott 1982, Harris *et al.* 1981).

STYLES OF FOLDING AND PENETRATIVE DEFORMATION

The main phase of penetrative deformation within the window is related to the emplacement of the Linville Falls and Tablerock thrust sheets (Boyer 1978). This penetrative deformation exhibits itself as 'metamorphic' or compositional layering in the basal arkose unit of the Grandfather Mountain Formation (Figs. 3 and 4).

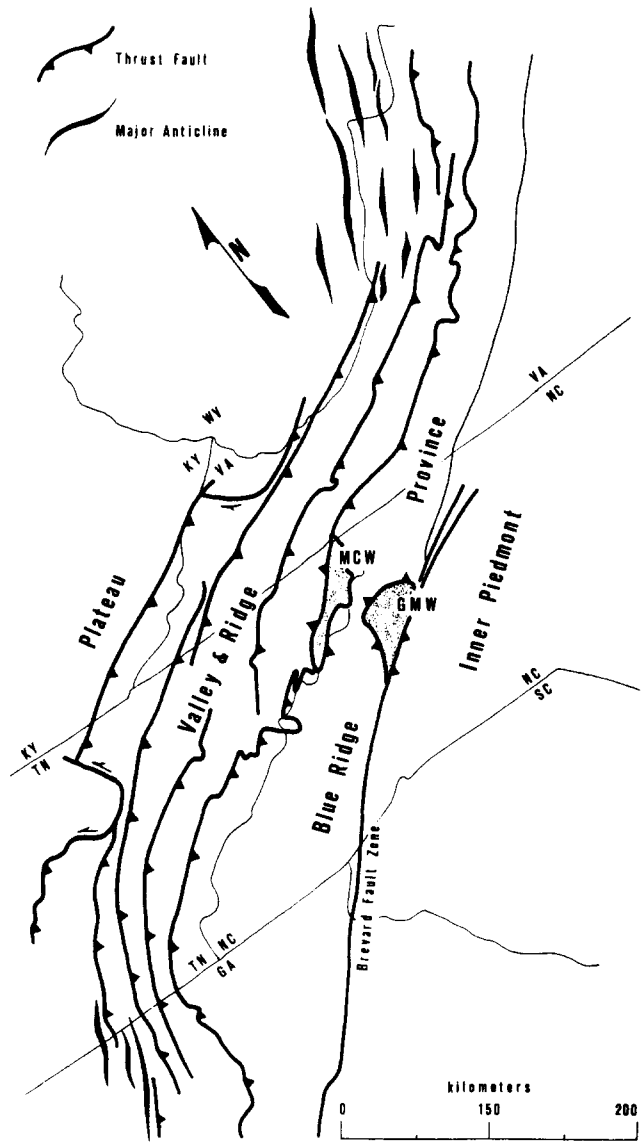

Fig. 1. The Grandfather Mountain Window (GMW) and Mountain City Window (MCW) are two large tectonic windows within the Blue Ridge Province of northeast Tennessee and northwest North Carolina. Compositional layering is developed in Late Precambrian arkoses of the Grandfather Mountain Window.

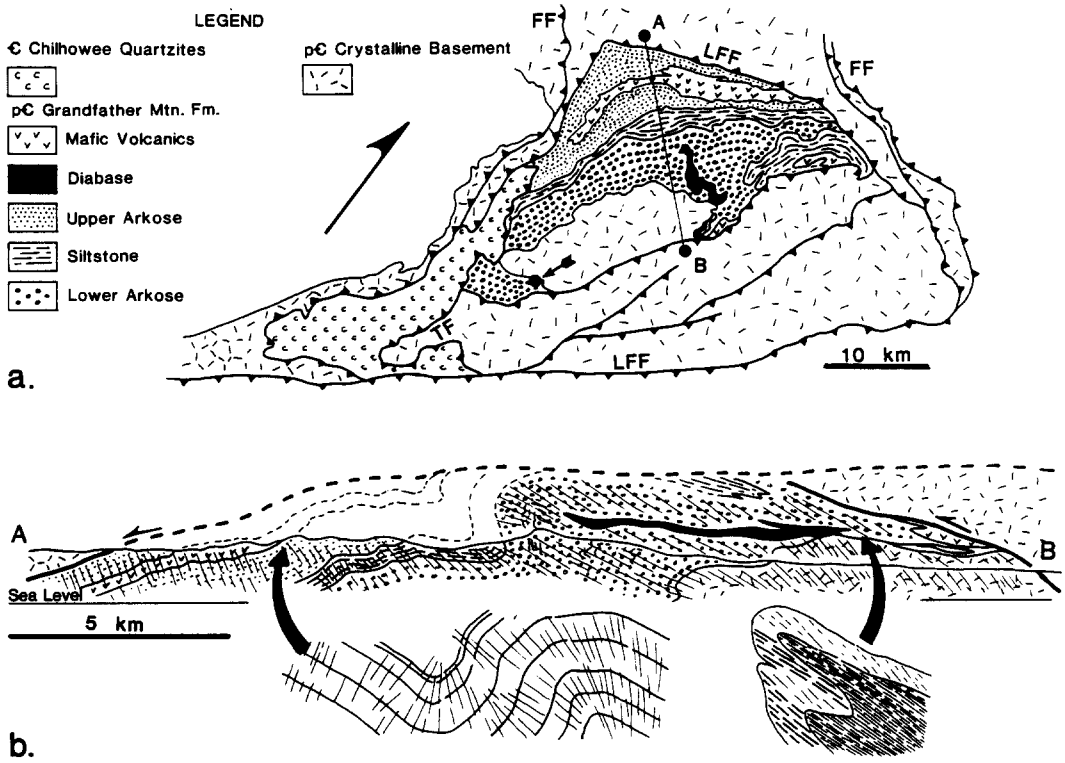

Fig. 2. (a) Geologic map of Grandfather Mountain Window. Unpatterned areas represent high-grade metamorphic rocks of possible equivalence to the Grandfather Mountain Formation. Arrow shows type locality for compositional layering and isoclinal folds (Figs. 3–9): major thrusts are the Linville Falls (LFF), Tablerock (TF) and Fries (FF). (b) Cross-section of the northwest Grandfather Mountain Window. Cleavage is at high angle to bedding in the northwest and decreases in dip toward the southeast. Inset figures show typical fold geometries in upper and lower arkoses.

The compositional layering is associated with tight to isoclinal folds in the basal arkose (Figs. 5 & 6). It is only sporadically developed in normal limbs, but occurs quite commonly in the overturned limbs. Layering in overturned limbs is approximately parallel to bedding in the upright limbs, whereas the average trend of the penetrative cleavage is oblique to the layering and defines the axial planes of folds.

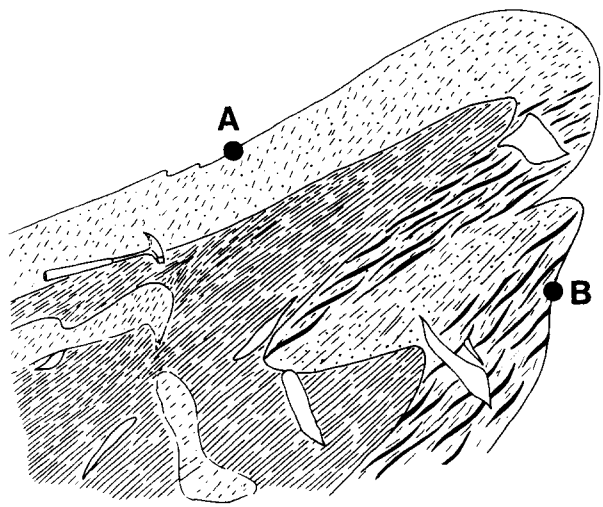

Fig. 5. Isoclinal fold in basal arkose. Compositional layers in overturned limbs are schematic; they are actually spaced less than 10 mm apart. Fold is cored by phyllitic siltstone. Note refraction of cleavage from siltstone to arkose in the upright limb. Unshaded irregular pods are quartz-filled fractures. Hammer is approximately 30 cm in length. Photomicrographs in Figs. 6(a) and (b) come from samples at A and B, respectively. Drawn from photographs.

The geometry of folds and the orientation and intensity of cleavage reflect a decrease in deformation from southeast to northwest (Fig. 2b). This decrease is accompanied by a change in deformation mechanisms. Towards the northwest and at higher structural levels, folds in the upper arkose unit are slightly overturned to asymmetric, upright and have a 'kink-style' or 'box-fold' geometry, similar to unmetamorphosed Valley and Ridge folds described by Faill (1973). A penetrative cleavage, defined by quartz pressure shadows and alignment of phengitic micas, fans about the folds at a high angle to bedding. Compositional layering is not present. The cleavage, which dips toward the southeast, increases in dip from southeast to northwest as isoclinal folds and compositional layering give way to open folds and fanning penetrative cleavage.

DESCRIPTION OF COMPOSITIONAL LAYERING

Layering in the basal arkoses consists of alternating feldspar-quartz domains, 5–10 mm thick, and mica folia, usually less than 1 mm thick (Figs. 3 and 7a). Although the mica folia often appear to be parallel to cleavage, closer examination reveals that cleavage in the feldspar–quartz domains is frequently at a significant angle to the mica folia (Figs. 4 and 7b).

The mica bands are of finite length, often less than 3 cm, and are arranged in en échelon fashion (Fig. 7b).

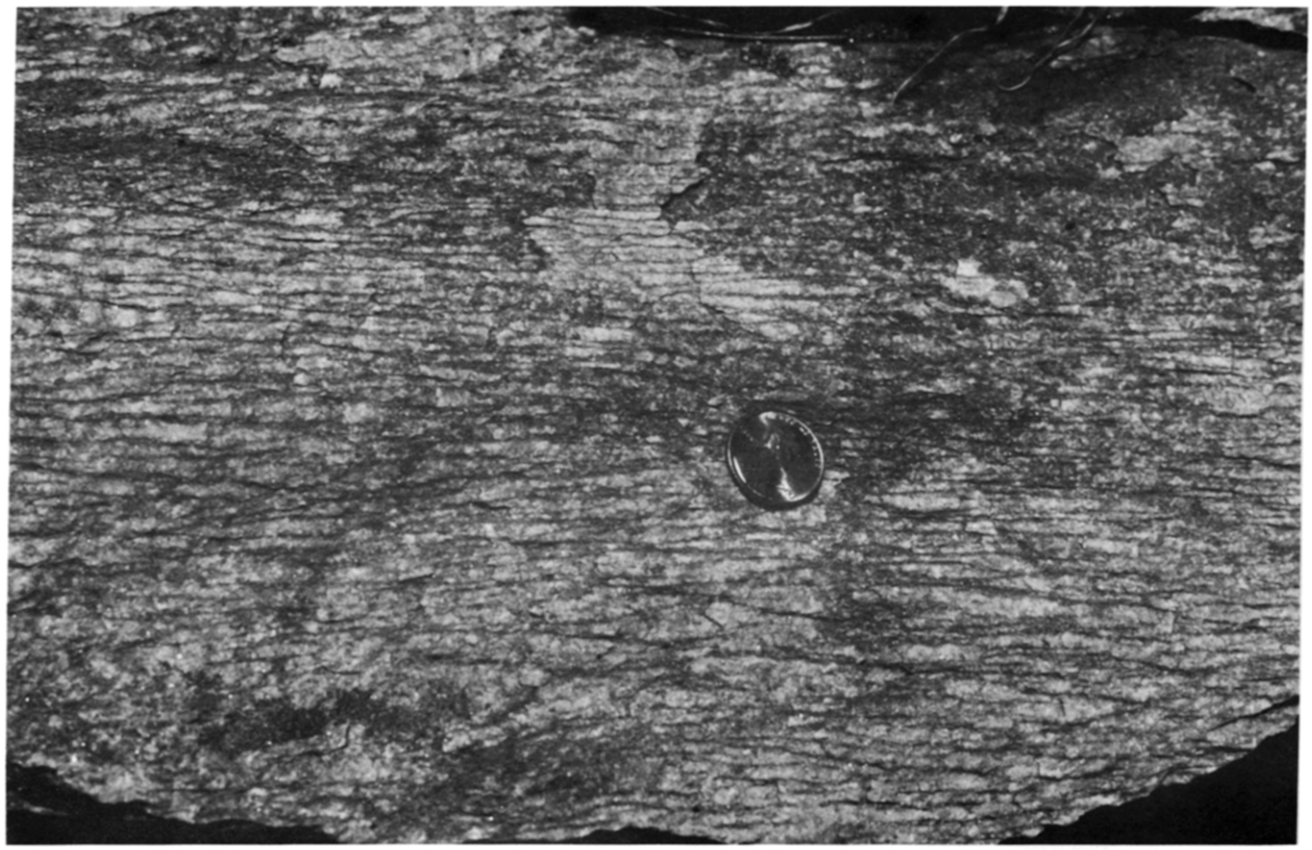

Fig. 3. Outcrop of compositional layering in basal arkose of the Grandfather Mountain Formation. Coin is U.S. penny (19 mm in diameter). Microscopic details of layering appear in Figs. 4 and 9.

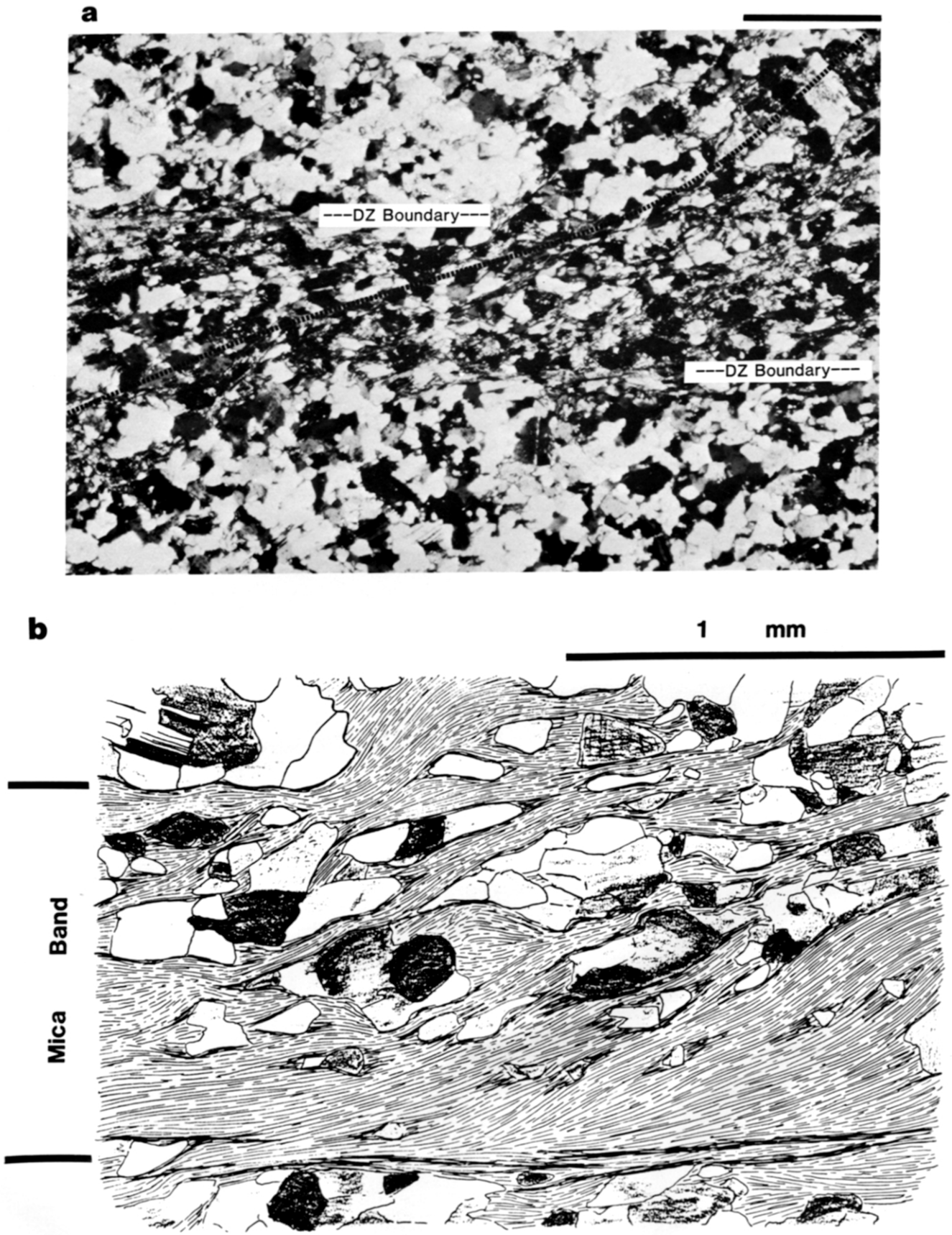

Fig. 4. (a) Photomicrograph of a mica band from outcrop shown in Fig. 3. Trajectory of cleavage is shown by dashed line. Bar scale = 1 mm. (b) Detail of mica alignment in the mica layer. Foliation is at an angle of 15° with the layer boundaries.

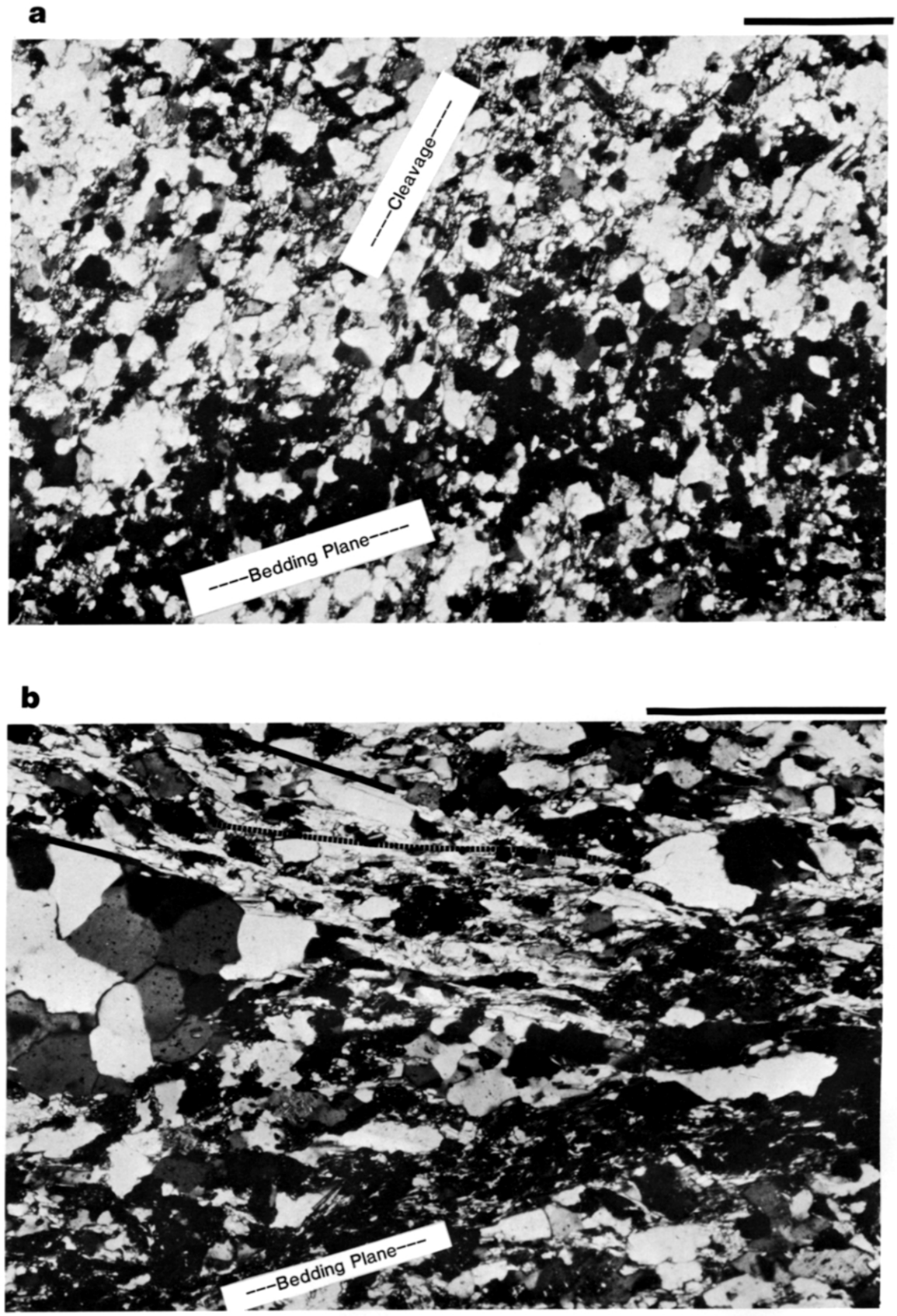

Fig. 6. (a) Photomicrograph of weakly developed cleavage in upright limb of fold shown in Fig. 5. Bar scale = 1 mm. (b) Junction of deformation zone and overturned bedding of fold shown in Fig. 5. Stratigraphic facing direction towards upper left. Dashed line shows trace of mica foliation which forms an angle of 14° with the zone boundaries (solid lines). Bedding plane and deformation zone form a conjugate shear set with right-lateral movement on the deformation zone and left-lateral movement on bedding. Bar scale = 1 mm (top right).

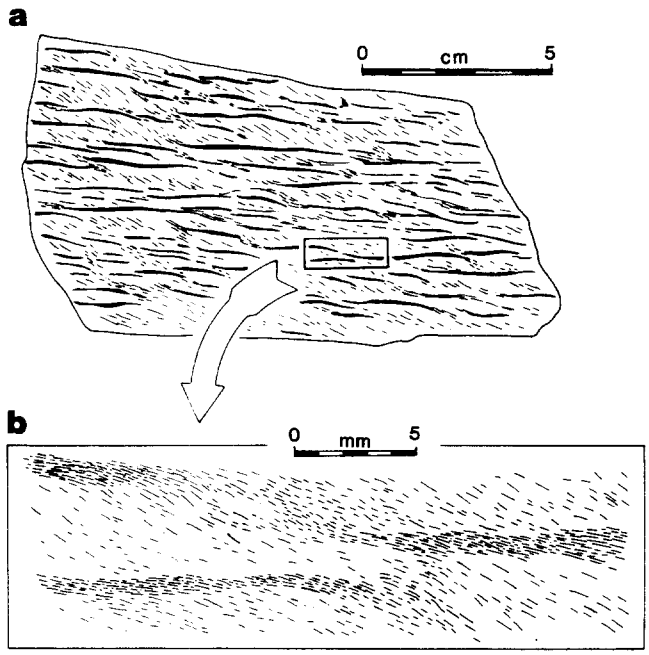

Fig. 7. (a) Drawing of compositional layering in cut and polished specimen from vicinity of fold shown in Fig. 5. Mica bands are horizontal and cleavage lies at an angle of approximately 27° to the foliation. (b) Drawing of photomicrograph showing mica alignments at junction of three mica folia. With respect to the layer boundaries, cleavage foliation forms an average angle of 11° in the mica bands and 27° in the quartz–feldspar domains.

The zones frequently terminate in 'horse-tails', diffuse zones of micro-cleavage which flare outward from the tips of the folia (Fig. 8a). The angle of the micro-cleavage to the folia increases as the folia terminate (Fig. 8b). Horse-tails may intertwine to connect two or more mica bands (Figs. 7 and 9).

The mica folia are depleted in quartz with respect to the quartz–feldspar domains. Point counts from thin-sections of the sample illustrated in Fig. 7(a) yielded the following percentages: in the mica folia, 6.8% quartz, 19.7% feldspar, 73.5% mica; and in the quartz–feldspar domains, 37.1% quartz, 14.2% feldspar and 48.7% mica.

The green mica is an iron-rich muscovite (Foster *et al.* 1960). Although a minor amount of the mica may have been derived from cataclasis and chemical decomposition of feldspar during deformation, most of it is probably the metamorphic product of original mica and clay (Bryant & Reed 1970, p. 79). This is suggested by the presence of unoriented phengitic micas in the matrix of undeformed arkose samples.

INTERPRETATION OF THE FABRICS AND THEIR SIGNIFICANCE

Boyer (1978, pp. 138–144, 1982) has interpreted the green mica folia as small-scale 'shear zones' (Ramsay & Graham 1970) or 'ductile deformation zones' (Mitra 1979), bands of rock which display higher strain values than adjacent material, which, in this case, are the quartz–feldspar bands. As do the larger deformation zones, they terminate in 'horse-tails', areas of increased deformation within the less-deformed 'country rock'. At the termination of a deformation zone, the shear strain, which was previously relegated to a narrow zone, is shared by a larger area of more uniform strain to produce the splayed 'horse-tail' structure (Ramsay 1976, Coward 1980, fig. 6, p. 23).

Often a horse-tail links two folia, serving to transfer slip from one to another (Fig. 9). Occasionally, the types of transfer combine to form a bifurcation (Fig. 7b). Thus the discontinuous en échelon segments can be considered to be part of a continuous deformation zone with several small steps, perhaps being analogous to the ramps and flats in thrust faults.

The compositional segregation of the deformation zones is the result of differential pressure solution during inhomogeneous deformation. In the incipient mica folia, pressure solution of quartz proceeded more rapidly than in the less deformed 'country-rock', the mica folia being depleted in quartz relative to the quartz–feldspar domains. Quartz lost by pressure solution found its way into fractures, forming the quartz veins which are ubiquitous in the Grandfather Mountain Formation. Some of the quartz derived from the mica folia may have precipitated as pressure shadows around clastic grains in the adjacent quartz–feldspar domains.

The relationship between the deformation zones and isoclinal folds (Fig. 5) suggests that folding in the basal arkose is the product of inhomogeneous shear strain along deformation zones and flexural slip along bedding. High shear strain parallel to bedding and deformation zones resulted in pressure-solution loss of quartz and the recrystallization and concentration of phengitic muscovite along bedding and deformation zones (Fig. 6b).

The overturned limbs of folds can be interpreted as mesoscopic deformation zones composed of yet smaller 1 mm thick deformation zones. Translation along the small-scale deformation zones assisted in the rotation of the overturned limbs and accompanied bedding-parallel slip in the upright limbs. S. Mitra (1978, p. 150) has previously suggested that ductile deformation zones have played an important role in the folding of Blue Ridge metasediments.

To date, most work on deformation zones has concentrated on those in crystalline basement. However, deformation zones may be more common in sedimentary rocks and low-grade metamorphosed sediments than previously recognized. If such is the case, one should use caution when using penetrative fabrics to unravel the structural history of multiply deformed rocks.

Schistosity in small-scale deformation zones lies at a smaller angle to deformation zone boundaries than does schistosity in adjacent, less-deformed bands, giving the misleading appearance of a penetrative fabric cut by a later crenulation cleavage. A single phase of inhomogeneous deformation can present a fabric similar to homogeneous, penetrative deformation followed by unrelated inhomogeneous deformation, thus leading one to postulate multiple deformational events when only one was operative.

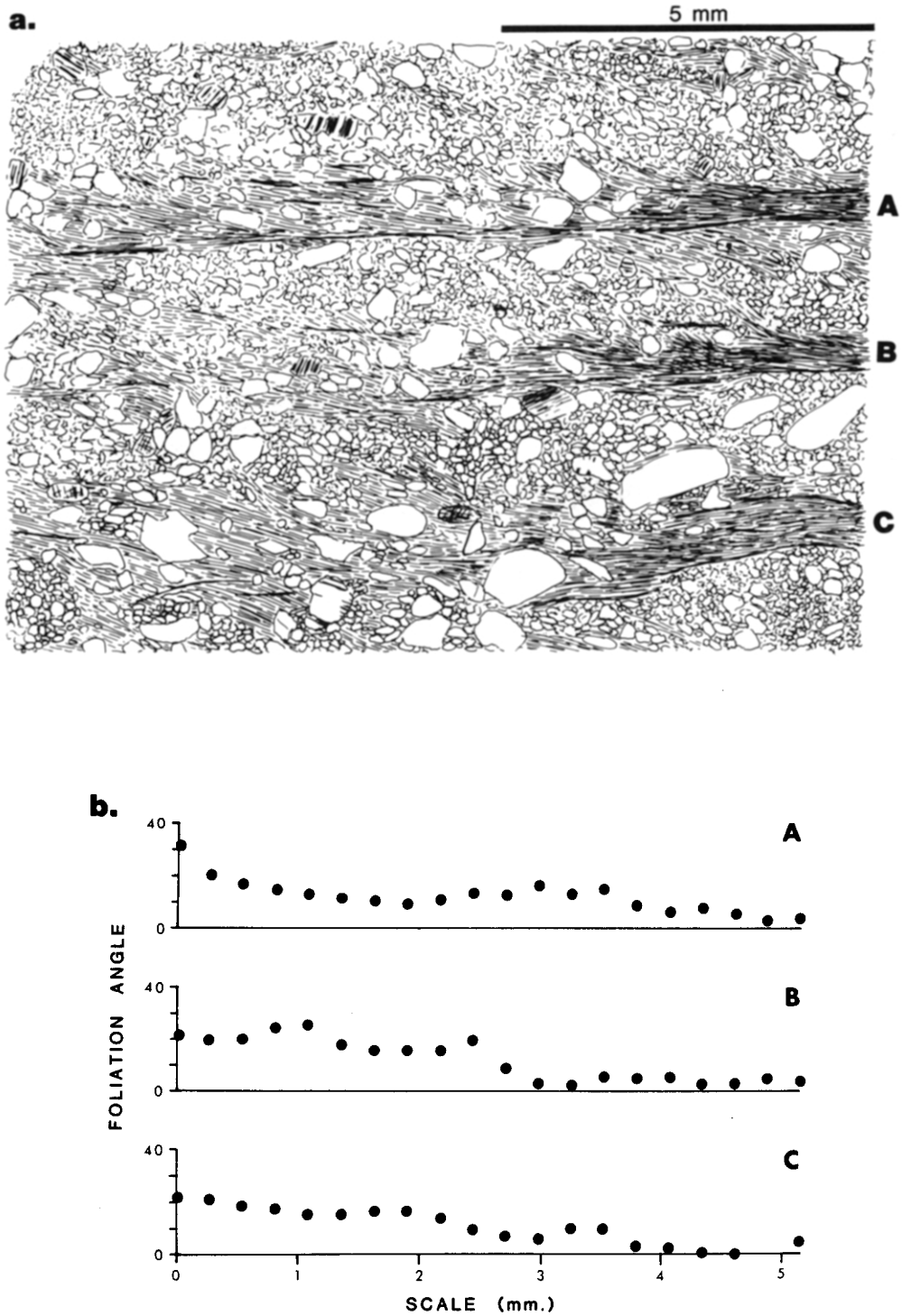

Fig. 8. (a) Three deformation zones (A–C). Lower two widen from right to left and terminate in 'horse-tails.' (b) Plots of foliation angles measured with respect to deformation zone boundaries, vs distance parallel to the boundaries. Cleavage angle increases as deformation zones terminate.

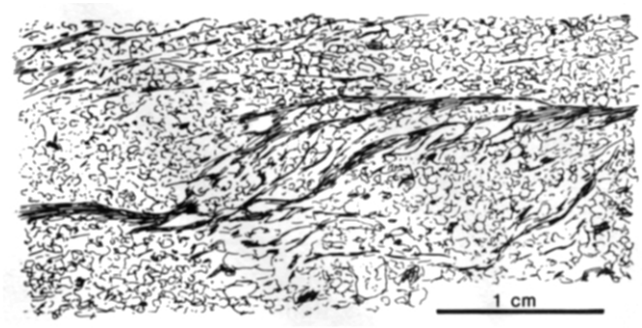

Fig. 9. Transfer zone between two deformation zones.

RELATIONSHIP BETWEEN DEFORMATIONAL STYLES IN CRYSTALLINE BASEMENT AND SEDIMENTARY COVER

The Grandfather Mountain Window permits a comparison of basement and cover deformation during greenschist–facies metamorphism. The style of deformation in the basal Grandfather Mountain Formation arkoses marks a transition from the formation of ductile

deformation zones in the underlying crystalline basement to folding in stratigraphically and structurally higher arkoses to the northwest (Boyer 1978, 1982a,b).

The basal arkoses are alluvial fan deposits, derived from adjacent basement highlands during Late Precambrian rifting. Being poorly bedded and mineralogically similar to the underlying basement, they deformed by the same mechanisms as the basement.

In the crystalline basement deformation is often concentrated in zones only a few millimeters thick, but larger deformation zones are mappable as distinct phyllonite zones (Bryant 1966, Bryant & Reed 1970). Near the contact with basement, deformation zones in the cover appear continuous with those in the basement, so that some folding in basal arkoses may owe its origin to displacement on deformation zones in the basement. As deformation and metamorphic grade decrease slightly at higher structural levels toward the northwest, deformation zones originating in the basement lose displacement. Shear strain is replaced by the horizontal shortening of upright, kink-style folds and fanning, high-angle cleavage. These conclusions on the relationship between basement and cover deformation are similar to those reached by Ramsay (1980, pp. 97–98). However, additional field study is required to evaluate the relationship of basement and cover deformation zones.

Deformation zones in the basal Grandfather Mountain Formation arkoses and adjacent crystalline basement present a rather simple pattern of en échelon subparallel zones at a low angle, usually less than 30°, to the penetrative cleavage. This simplicity is in contrast to the complex patterns of deformation zones in basement rocks of the Blue Ridge Province of northern Virginia (Mitra 1979). Mitra (1979, p. 947) identified four octahedral sets, a set parallel to cleavage, and a set perpendicular to cleavage, all at high angles to the horizontal, and a subhorizontal set. The deformation zones observed by Mitra formed at lower to middle greenschist–facies metamorphism (G. Mitra 1978, p. 1059), whereas the deformation zones in basal Grandfather Mountain arkoses formed at upper greenschist facies (Rankin *et al.* 1972). The deformation zones in the northern Blue Ridge formed in a regime of horizontal shortening (estimated at 52%; Mitra 1979), while those in the southern Blue Ridge reflect large horizontal shear strain components associated with emplacement of major thrust sheets of Precambrian crystalline basement.

STRAIN WITHIN DEFORMATION ZONES

Deviatoric natural strain within the deformation zones and the less deformed quartz–feldspar domains is a function of natural strain, ϵ_{11}, parallel to the boundaries of the deformation zones, the angle, θ, that the penetrative fabric makes with the walls of the folia, and ϵ_A, the natural area strain (assuming plane strain):

$$\epsilon_d = 1/2 \ln \left\{ \left[\frac{1 + \cos 2\theta}{(\cos 2\theta - 1)\exp(4\epsilon_A)} + \left(\frac{\exp(-2\epsilon_{11})}{\cos 2\theta - 1} \right)^2 \right]^{1/2} - \left[\frac{\exp(-2\epsilon_{11})}{\cos 2\theta - 1} \right] \right\} [\exp(2\epsilon_A)]. \quad (1)$$

(See Appendix for derivation of this equation and an explanation of strain measures.)

Figure 11 shows the variation in ϵ_d with θ for various area strains, ϵ_A, in cases where there is no elongation or shortening parallel to the boundary of a deformation zone. The curve for $\epsilon_A = 0$ is the special case of simple shear.

A plot of ϵ_d vs θ for $\epsilon_A = 0$ and various ϵ_{11} produces a similar set of curves (Fig. 12). Since we are dealing in plane strain, the volume loss is represented by area change in the principal plane.

As a first approximation let us assume that there is no area change in the quartz–feldspar domain, that is $\epsilon_A = 0$. The relationship of the deformation zones to folds suggests that any strain parallel to the deformation zones will be elongation, $\epsilon_{11} > 0$. From Fig. 12 we can see that the maximum value of strain can be determined from the curve for $\epsilon_{11} = 0$. In my description (Fig. 7), I stated that the average angle of cleavage in the quartz–feldspar domains of our sample was 27°. From equation (1) we find that a maximum $\epsilon_d = 0.67$. In terms of axial ratios, AR = 3.82 (ϵ_d = 1/2 ln AR).

In the mica, folia strain was approximated by comparing the amount of quartz relative to feldspar and mica in the mica folia and quartz–feldspar domains. In the sample modal counts of 500 grains in three mica folia and 500 grains in three quartz–feldspar domains yielded the following average percentages.

	Quartz	Feldspar	Mica
Mica folia	6.8	19.7	73.5
Quartz–feldspar domains	37.1	14.2	48.7

The ratio of feldspar to mica is 0.27 in the mica folia and 0.29 in the quartz–feldspar domain. These modes can be explained by pressure solution removal of quartz from the mica folia, indicating an area change of $\Delta = -0.34$, where Δ is the change in area divided by the original area, or in terms of natural area strain ($\epsilon_A = 1/2 \ln(\Delta + 1)$), $\epsilon_A = -0.21$.

If $\epsilon_A = -0.21$ and $\theta = 11°$ in the mica folia (Fig. 7), from equation (1) we calculate that the maximum strain in the folia would be $\epsilon_d = 1.40$ (AR = 16.44).

We can see from Figs. 12 and 13 that with increasing strain the angle θ decreases. It was stated previously that in some cases the angle between cleavage and the mica folia was too small to measure and that in many cases the cleavage appeared to be parallel to the folia. This situation could be explained by high values of shear strain.

CONCLUSIONS

Mica bands in the basal arkose unit of the Grandfather Mountain Formation are small-scale deformation zones. They are 1 mm thick and spaced 5–10 mm apart by less-deformed quartz–feldspar layers. Folding in the poorly bedded basal arkose was achieved by a combination of flexural slip and translation along deformation zones in the overturned limbs. Tight folds and deformation zones in the basal arkoses mark a deformational style transitional between the formation of ductile deformation zones in the underlying basement and open, kink-style folds at higher structural and stratigraphic levels in the cover.

Assuming plane strain, strain ellipse axial ratios are approximately 4:1 in the quartz–feldspar domains and 16:1 in the mica bands. If strain in the quartz–feldspar layers was achieved with little or no area change, strain in the mica bands was accompanied by a 34% loss of area due to pressure solution removal of quartz. Pressure-solved quartz filled adjacent fractures.

Small-scale deformation zones can give the misleading appearance of a penetrative cleavage cut by a later crenulation or 'strain-slip' cleavage. This could lead investigators to postulate two or more deformational events when only one is present.

In light of these conclusions it might prove useful to re-examine rock specimens which have led many researchers to suggest that at least some forms of cleavage represent planes of high shear strain. The deformation zones I have described are quite small and closely spaced, and since the rock parts along the deformation zones, as well as along the higher-angle cleavage in the quartz–feldspar domains, the rock could be described as having two cleavages. If previous workers were indeed describing small-scale deformation zones, which they may have termed cleavage, they would have been correct in ascribing 'shear' to the origin of such cleavages.

Acknowledgements—This paper is a portion of a Ph.D. thesis completed in 1978 under the guidance of Dr. David Elliott at the Johns Hopkins University. I wish to dedicate this paper to the memory of Dave, without whose constant reassurance, advice, and encouragement, neither this paper nor my thesis would have been completed. I wish also to thank Dr. Gautam Mitra for his advice and constructive criticism and his assistance in the field on several occasions.

Field work was supported by grants from the Geological Society of America and Sigma Xi and by funds from a National Science Foundation grant (NSF DES74-17647) awarded to Dr. David Elliott. The Department of Earth and Planetary Sciences of the Johns Hopkins University provided assistance through the Balk Fund.

REFERENCES

Boyer, S. E. 1976. Formation of the Grandfather Mountain Window, North Carolina, by duplex thrusting. *Geol. Soc. Am. Ann. meeting (1976) with abs.* **9**, 788–789.

Boyer, S. E. 1978. Structure and origin of Grandfather Mountain Window, North Carolina. Unpublished thesis, Johns Hopkins University, Baltimore, Maryland.

Boyer, S. E. 1982a. Penetrative deformation in crystalline basement and Late Precambrian sediments, Grandfather Mountain and vicinity, North Carolina. *Geol. Soc. Am. Abs.* Northeastern and Southeastern Combined Sect. Mtgs. **14**, 7.

Boyer, S. E. 1982b. Origin and significance of compositional layering in Late Precambrian sediments, North Carolina. *Mitt. Geol. Inst. ETH Univ. Zürich* **239a**, 43–46.

Boyer, S. E. & Elliott, D. 1982. Thrust systems. *Bull. Am. Ass. Petrol. Geol.* **66**, 1196–1230.

Bryant, B. 1966. Formation of phyllonites in the Grandfather Mountain area, northwestern North Carolina. *Prof. Pap. U.S. geol. Surv.* **550D**, D144–D150.

Bryant, B. & Reed, J. C. 1970. Geology of the Grandfather Mountain Window and vicinity, North Carolina and Tennessee. *Prof. Pap. U.S. geol. Surv.* **615**.

Coward, M. P. 1980. Shear zones in the Precambrian crust of Southern Africa. *J. Struct. Geol.* **2**, 19–28.

Elliott, D. 1970. Determination of finite strain and initial shape from deformed elliptical objects. *Bull. geol. Soc. Am.* **31**, 2221–2236.

Faill, R. T. 1973. Kink-band folding, Valley and Ridge Province, Pennsylvania. *Bull. geol. Soc. Am.* **84**, 1289–1314.

Foster, M. D., Bryant, B. & Hathaway, J. 1960. Iron-rich muscovitic mica from the Grandfather Mountain area, North Carolina. *Am. Miner.* **45**, 839–851.

Harris, L. D., Harris, A. G., de Witt, Jr., W. & Bayer, K. C. 1981. Evaluation of southern Eastern Overthrust Belt beneath Blue Ridge–Piedmont thrust. *Bull. Am. Ass. Petrol. Geol.* **65**, 2497–2505.

Jaeger, J. C. 1969. *Elasticity, Fracture, and Flow*. Methuen, London.

Mitra, G. 1978. Ductile deformation zones and mylonites: the mechanical processes involved in the deformation of crystalline basement rocks. *Am. J. Sci.* **278**, 1057–1084.

Mitra, G. 1979. Ductile deformation zones in Blue Ridge basement rocks and estimation of finite strains. *Bull. geol. Soc. Am.* **90**, 935–951.

Mitra, S. 1978. Microscopic deformation mechanisms and flow laws in quartzites within the South Mountain Anticline. *J. Geol.* **86**, 129–152.

Nicholson, R. 1968. On kink-zone development and metamorphic differentiation in the low-grade schists of Norwegian Sulitjelma. *Norges geol. Unders.* **247**, 133–146.

Ramsay, J. G. 1967. *Folding and Fracturing of Rocks*. McGraw-Hill, New York.

Ramsay, J. G. 1976. 1st Annual Ernst Cloos Memorial Lectures (unpublished). Johns Hopkins University, Baltimore.

Ramsay, J. G. 1980. Shear zone geometry: a review. *J. Struct. Geol.* **2**, 83–100.

Ramsay, J. G. & Graham, R. H. 1970. Strain variation in shear belts. *Can. J. Earth Sci.* **7**, 786–813.

Rankin, D. W., Espenshade, G. H. & Neuman, R. B. 1972. Geologic map of the west half of the Winston-Salem quadrangle, North Carolina, Virginia, Tennessee. *U.S. geol. Surv. Misc. Geol. Inv.* **Map I-709A**.

Talbot, J. L. & Hobbs, B. E. 1968. The relationship of metamorphic differentiation to other structural features at three localities. *J. Geol.* **76**, 581–587.

Voll, G. 1960. New work on petrofabrics. *Lpool Manchr geol. J.* **2**, 503–567.

Williams, P. F. 1972. Development of metamorphic layering and cleavage in low-grade metamorphic rocks at Bermagui, Australia. *Am. J. Sci.* **272**, 1–47.

APPENDIX

Calculation of strain in deformation zones

Assuming plane strain, I will derive an equation that will give the deviatoric natural strain, ϵ_d, in terms of θ, the angle that cleavage makes with the deformation zone boundary, ϵ_A, the natural area strain during deformation, and ϵ_{11}, the natural strain parallel to the deformation zone boundary

$$\epsilon_d = f(\theta, \epsilon_{11}, \epsilon_A).$$

The x_1 reference axis is oriented parallel to the deformation zone boundary and x_2 perpendicular to the boundary. θ is the angle between the principal elongation axis of the strain ellipse and the x_1 reference axis (Fig. 10).

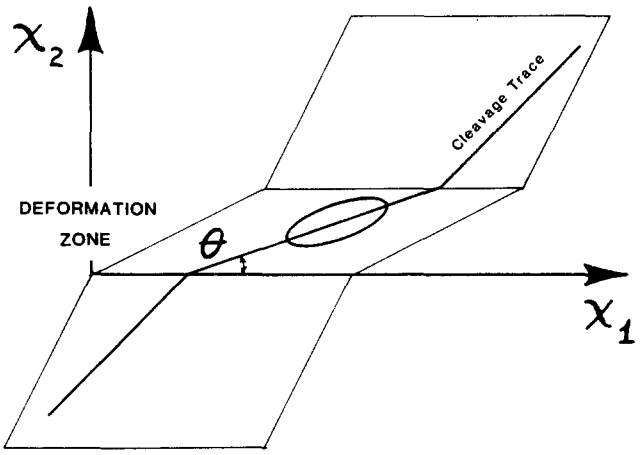

Fig. 10. Reference frame for strain calculations from deformation zones. Plane strain is assumed. X_1 is oriented parallel to zone boundaries. The trace of foliation in the principal plane is assumed to represent the principal elongation axis, which forms an angle of θ with the deformation zone boundaries.

Solving equation 3-49 of Ramsay (1967, p. 69) for the maximum inverse quadratic elongation,

$$\lambda_1' = \frac{\lambda_2'(\cos 2\theta - 1) + 2\lambda_{11}'}{1 + \cos 2\theta}, \tag{1}$$

where λ_2' is the minimum inverse quadratic elongation and λ_{11}' is the inverse quadratic elongation parallel to the deformation zone boundary. The relationship of area change to inverse longitudinal strains is

$$\frac{1}{(\Delta + 1)^2} = \lambda_1'\lambda_2'$$

(derived from Jaeger 1969, eq. §18(5) or Ramsay 1967, eq. 3-27). Therefore

$$\lambda_1' = \frac{1}{\lambda_2'(\Delta + 1)^2}. \tag{2}$$

Substituting this value for λ_1' into equation (1) and solving for λ_2' we arrive at

$$\lambda_2' = \left[\frac{1 + \cos 2\theta}{(\Delta + 1)^2(\cos 2\theta - 1)} + \left(\frac{\lambda_{11}'}{\cos 2\theta - 1}\right)^2\right]^{1/2} - \left[\frac{\lambda_{11}'}{\cos 2\theta - 1}\right]. \tag{3}$$

Dividing λ_2' by λ_1' (equation 2),

$$\frac{\lambda_2'}{\lambda_1'} = (\lambda_2')^2(\Delta + 1)^2.$$

Replacing λ_2' on the right side of this equation by the equivalent of λ_2' in equation (3),

$$\frac{\lambda_2'}{\lambda_1'} = \left\{\left[\frac{1 + \cos 2\theta}{(\Delta + 1)^2(\cos 2\theta - 1)} + \left(\frac{\lambda_{11}'}{\cos 2\theta - 1}\right)^2\right]^{1/2} - \left[\frac{\lambda_{11}'}{\cos 2\theta - 1}\right]\right\}^2 (\Delta + 1)^2. \tag{4}$$

Deviatoric natural strain can be defined by

$$\epsilon_d = 1/2 \ln (\lambda_2'/\lambda_1')^{1/2}$$

(derived from eq. §18(4), Jaeger 1969). Therefore, from equation (4) we define

$$\epsilon_d = 1/2 \ln \left\{\left[\frac{1 + \cos 2\theta}{(\Delta + 1)^2(\cos 2\theta - 1)} + \left(\frac{\lambda_{11}'}{\cos 2\theta - 1}\right)^2\right]^{1/2} - \left[\frac{\lambda_{11}'}{\cos 2\theta - 1}\right]\right\} (\Delta + 1). \tag{5}$$

Let us rewrite this equation, converting all terms to natural strain measure.

We know that

$$\lambda = \exp(2\epsilon) \tag{6}$$

(Jaeger 1969, eq. 18(4)). Therefore, in (1)

$$\lambda_{11}' = \exp(-2\epsilon_{11}). \tag{7}$$

$$\Delta = (\lambda_1\lambda_2)^{1/2} - 1 \tag{8}$$

(Jaeger 1969, eq. 18(5)). Applying (6) to (8) we derive

$$\Delta = \exp(\epsilon_1 + \epsilon_2) - 1. \tag{9}$$

Since

$$\epsilon_1 + \epsilon_2 = 2\epsilon_A \tag{10}$$

where ϵ_A is the natural area strain (Elliott 1970),

$$\Delta = \exp(2\epsilon_A) - 1. \tag{11}$$

Using (7) and (11) we write (5) entirely in terms of natural strains:

$$\epsilon_d = 1/2 \ln \left\{\left[\frac{1 + \cos 2\theta}{(\cos 2\theta - 1)\exp(4\epsilon_A)} + \left(\frac{\exp(-2\epsilon_{11})}{\cos 2\theta - 1}\right)^2\right]^{1/2} - \left[\frac{\exp(-2\epsilon_{11})}{\cos 2\theta - 1}\right]\right\} [\exp(2\epsilon_A)]. \tag{12}$$

From this equation, I constructed two graphs to express the variation of θ with ϵ_d for certain values of ϵ_A and ϵ_{11}. The first graph (Fig. 11) is a plot of ϵ_d vs θ for various ϵ_A and a fixed ϵ_{11}. The second (Fig. 12) shows how strain along the boundary of a deformation zone affects the relationship between ϵ_d and θ for a fixed ϵ_A.

Portions of these curves represent unreal strain situations, reflecting the fact that in these calculations we are treating the finite strain state as the result of three independently imposed strains: (1) elongation parallel to the DZ boundary, ϵ_{11}; (2) simple shear parallel to the DZ boundary; and (3) area strain, ϵ_A. To understand why portions of these curves are 'imaginary' let us consider a hypothetical example.

Please refer to Fig. 11. Consider the curve for $\epsilon_A = -0.35$ ($\Delta = -0.50$). This curve expresses the relationship between ϵ_d and θ, where there is no strain parallel to the DZ boundary, $\epsilon_{11} = 0$, and there is no area strain.

The left end of this curve is anchored at the point (0.347, 0). This is the initial state, before any shear strain has been applied. As shear strain is added, ϵ_d increases and θ initially increases. However, θ does not exceed 20°, and beyond $\epsilon_d = 0.7$ it begins to decrease.

The actual strain history of a deforming rock would not follow one of these curves, however. We are considering deformation zones in which area loss by pressure solution proceeds as a result of shear strain. In the initial state $\epsilon_A = 0$. For example, if shear stresses are applied to a rock, the rock does not lose 50% of its volume until it has undergone a great deal of shear strain.

Therefore, it is assumed that for curves of $\epsilon_A < 0$, that portion of any curve to the left of the curve's peak is unreal. For real situations θ will decrease with increasing strain; it will never increase. A possible real strain history for a deformation zone is shown in Fig. 13. Note that $\epsilon_{11} = 0$, that is there is no shortening or elongation parallel to the direction of shear.

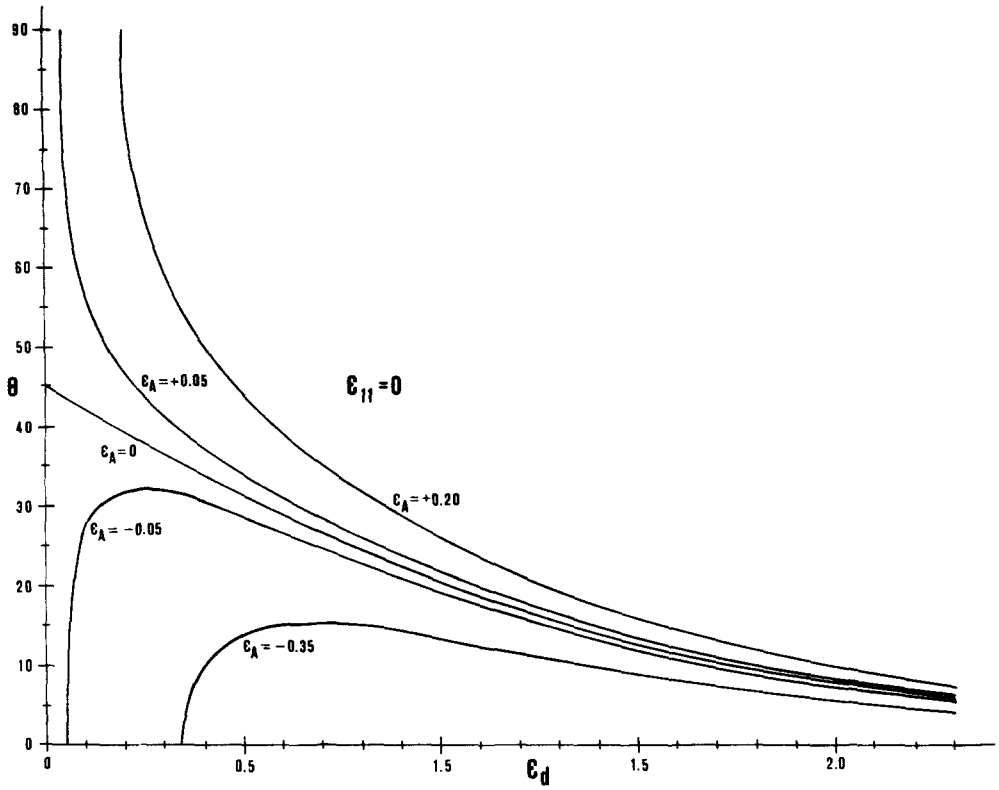

Fig. 11. Plot of cleavage orientation vs deviatoric natural strain for various values of area change and for cases in which there is no elongation or shortening parallel to the deformation zone boundaries.

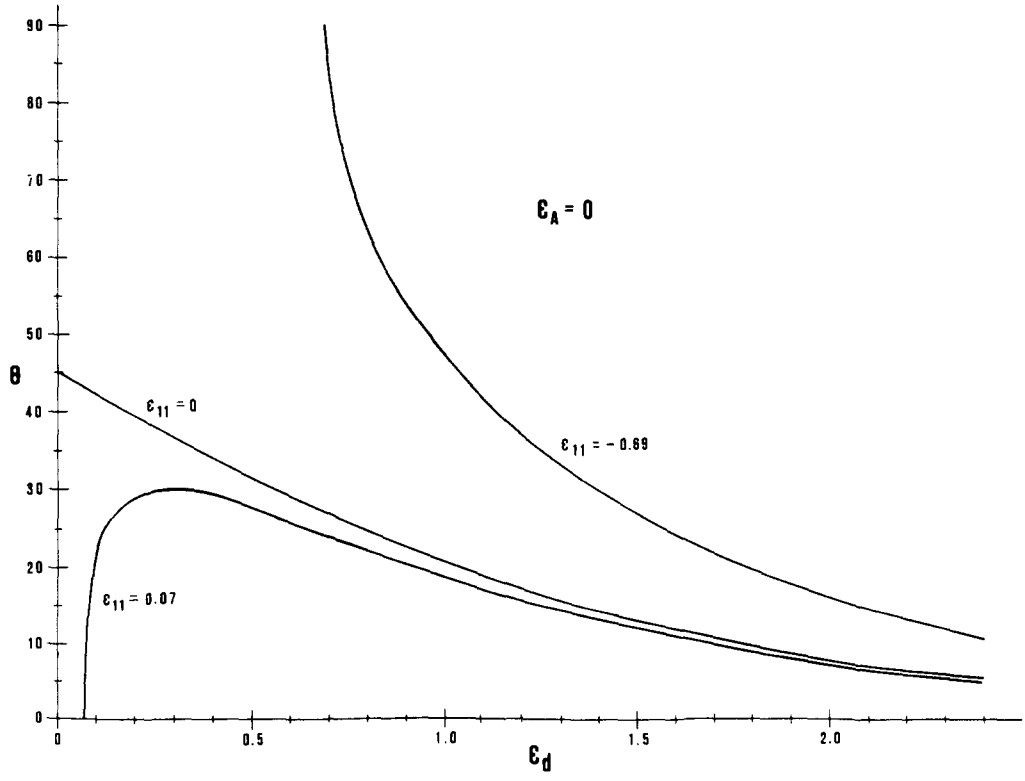

Fig. 12. Variation of deviatoric natural strain with cleavage angle for inverse longitudinal elongations of −0.69, 0 and 0.07 parallel to the deformation zone boundaries. No area change.

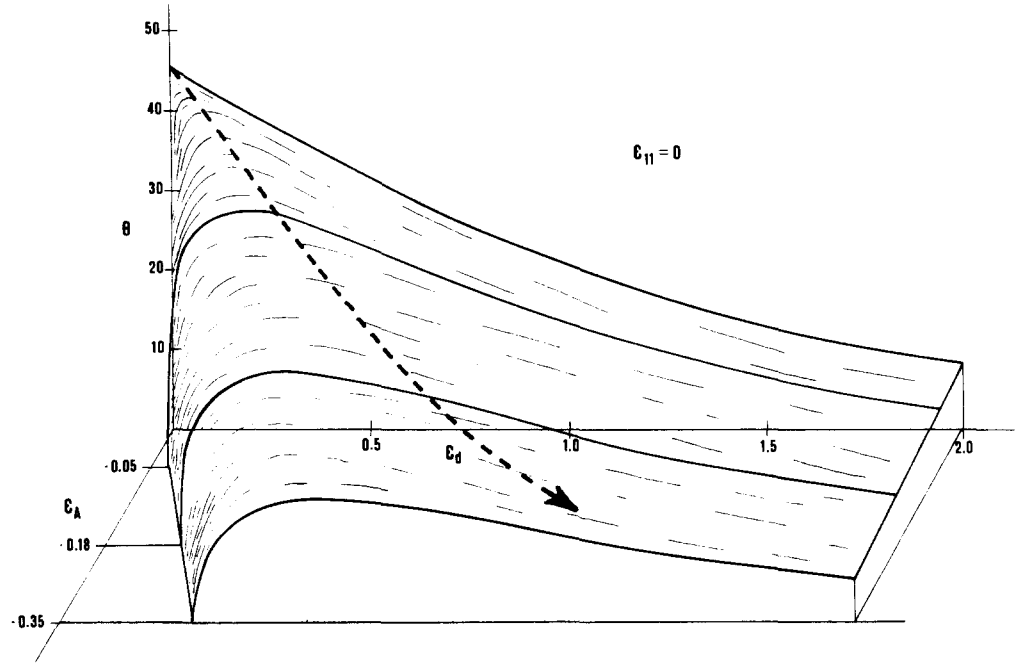

Fig. 13. Possible deformation history (dashed line) within an evolving deformation zone in which there is no change in dimensions parallel to the deformation zone boundaries. Axes are: θ, the angle of cleavage; ϵ_A, the natural area strain; and ϵ_d, deviatoric natural strain.